Journal of Applied Fluid Mechanics, Vol. 14, No. 3, pp. 779-792, 2021.
Available online at www.jafmonline.net, ISSN 1735-3572, EISSN 1735-3645.
DOI: 10.47176/jafm.14.03.31857

Computational and Experimental Investigations of Separation Control of LP Turbine Cascade Blades using Gurney Flaps

G. Tatpatti[1], N. Sitaram[2†] and K. Viswanath[2]

[1] *Department of Mechanical Engineering, R. V. College of Engineering, Mysuru Road, R. V. Vidyanikethan Post, Bengaluru - 560059, India*
[2] *Department of Mechanical Engineering, Indian Institute of Technology Madras, Chennai – 600036, India*

[†]*Corresponding Author, Email: nsitaram.iitm@gmail.com*

(Received May 26, 2020; accepted October 8, 2020)

ABSTRACT

The paper reports computational and experimental investigations carried out to control of laminar flow separation in LP turbine cascade blades at low Reynolds numbers. T106 LP turbine blade profile with a chord of 60 mm and blade spacing of 48 mm was used. The blade Zweifel loading factor was 1.03. Passive separation control device of Gurney flaps (GFs) of different shapes and sizes were used. Computations were carried out in Ansys-CFX. A two-equation eddy-viscosity turbulence model, shear stress transport (SST) was considered for all the computations along with gamma-theta (γ–θ) transition model. Computations were carried out for five different Reynolds numbers. Lift coefficient, total pressure loss coefficient, overall integrated loss coefficient and ratio of lift coefficient to overall integrated loss coefficient were used as a measure of aerodynamic performance for the cascade. From the computations, Flat and Quarter Round GFs of heights of 1.33% of chord were identified as the best configurations. Experiments in a seven bladed cascade were carried out for these configurations along with the basic configuration without GF at five Reynolds numbers. Experimental results agreed well with the computational results for these three cases at the five Reynolds numbers.

Keywords: LP turbine cascade; Gurney flap; Separation control; Computational investigations; Experimental investigations.

NOMENCLATURE

C	velocity
Ch	chord
Ch_x	axial chord
C_L	lift coefficient
C_P	static pressure coefficient on blade surfaces
h	Gurney flap height
H	Gurney flap height as a percentage of chord
P	static pressure
Re	Reynolds number
X	non-dimensional axial distance
x	axial distance from leading edge
Y	non-dimensional pitchwise distance
y	pitchwise distance from trailing edge
y	distance to the nearest wall
y^+	non-dimensional distance from the wall
y^+_{min}	minimum value of y^+
u*	friction velocity
ν	kinematic viscosity
ρ	density
Ψ_{in}	overall integrated loss coefficient
ψ	total pressure loss coefficient
0	total conditions
1, 2	cascade inlet and outlet respectively

Abbreviations

FF	Flat
GF	Gurney Flap
HR	Half Round
QR	Quarter Round
TR	Triangular

1. INTRODUCTION

Gas turbines used in aero engine consists of a fan, LP compressor (5-6 stages), HP compressor (9-10 stages), combustion chamber, HP turbine (2 stages) and LP turbine (6-7 stages). The weight of LP turbine is nearly 30% of engine weight and the LP turbine contains as high as 1900 individual blades (Curtis *et al.* 1997). The aerodynamic performance of the LP turbine is dependent on various parameters like Reynolds number, incidence and blade angle. LP turbines in aircraft engines undergo tremendous losses at cruise conditions. Gas turbine engines are mainly designed to perform better at high Reynolds numbers, especially during takeoff and landing. But during high altitude cruise, in thin air conditions and low velocities, Reynolds numbers in LP turbines can fall as low as 25000. Sharma (1998) found that total pressure loss coefficient increases from around 0.03 to 0.10 with the decrease in Reynolds number. Even for the modern engine requirements which includes further high altitude flight of unmanned air vehicles (UAV) and also to reduce the number of airfoil count in the existing LP turbines to reduce engine cost and weight, the current state of LP turbine pose more challenges. However as the blade number is decreased, solidity decreases, flow separation is likely to increase total pressure losses. Hence there is a need to reduce flow separation using active or passive devices.

At low Reynolds number in an LP turbine airfoil, Baneighbal *et al.* (1995) found that 60% of losses occur on suction surface. This abrupt increase of total pressure loss at low Reynolds numbers is mainly attributed to laminar separation of flow on the suction surface of the blade. Hence there is a need to control the laminar flow separation on LP turbine blade to decrease the total pressure loss coefficient at low Reynolds numbers as well as to meet the increasing demands of further higher altitude cruise and decreasing the blade count for LP turbine.

Gurney flap (GF) is one such simple passive device to prevent laminar flow separation. A Gurney flap is a short, flat plate attached perpendicular to the pressure side of an airfoil near the trailing edge. The deflection of the cascade mainstream due to Gurney flap can accelerate the flow at suction side of the adjacent blade, and decrease the adverse pressure gradient which delay the laminar separation and delay transition onset, which in turn leads to reduction in loss due to separation bubble and turbulent boundary layer. Gurney flap also enhances the lift generated by an individual airfoil because of the increase in effective camber. Gurney flap is extensively used in improving the performance of airfoils. Wang *et al.* (2008) presented a comprehensive review of Gurney flap applications to airfoils. However, application of Gurney flap to turbomachinery is limited.

2. MOTIVATION

Many active and passive devices have been used to control the laminar separation on the suction surface of LP turbine cascade blade. Active flow control devices require an additional source of energy for operation. Sondergaard *et al.* (2002) used an active flow control device namely steady vortex generator jets and found that the total pressure loss coefficient was reduced by a factor of 2-3. Volino and Ibrahim (2012) used pulsating vortex generator jets which showed increase in lift coefficient by 20% and decrease in wake loss by 60% at low Reynolds numbers. Chen *et al.* (2010) used jet flap on the pressure side of the blade near the trailing edge and found that cascade solidity can be decreased by 12.5%. Active flow control system has the advantage of deactivating itself when LP turbines are operating at higher Reynolds numbers. The disadvantage of all these active control devices is the practicality in actual turbine engine environment.

Passive flow control devices do not require an additional source of energy for their operation. Lake *et al.* (1999) used dimples on suction surface and found that the loss coefficient got reduced by 50%. Volino (2003) used rectangular bars on suction surface to eliminate the boundary layer separation. There have been only few previous investigations of Gurney flap in turbomachinery application. Most of the previous work on Gurney flap was on airfoils and wings. Byerley *et al.* (2003) used Gurney flap to control the laminar flow separation experimentally. Recently Nilavarasan *et al.* (2019) performed computational investigations on NACA 0010 cascade using Gurney Flaps with different inclinations at different stagger angles. Dundi *et al.* (2012) experimentally demonstrated that application of Gurney flap to the tip of a centrifugal impeller blade improves the performance at low Reynolds number. Suresh and Sitaram (2019) tested the same centrifugal fan with three types of Gurney flaps, angle, quarter round and half round types of different heights at different Reynolds numbers and found that quarter round Gurney flap gives slightly improved performance compared to the other two types. However, the investigations on Gurney flap for turbomachinery are very limited. Hence there is a need to study the effect of Gurney flap on the performance on the LP turbine cascade by varying various parameters like height, shape of Gurney flap and operating Reynolds numbers.

3 OBJECTIVES AND SCOPE

The present paper aims to study the effect of Gurney flap on the LP turbine cascade performance at low Reynolds numbers, which is susceptible to flow separation because of large flow turning angle. Initially the effect of Reynolds number is studied on the baseline case. The performance parameters chosen for analysis are static pressure distribution over the blade surface, total pressure loss

coefficient (ψ), lift coefficient (C_L) and overall integrated loss coefficient (ψ_{int}). Computational analysis is carried out by systematically varying the height and configuration of Gurney flap. Based on the performance of the GF, the best configurations are selected. Experimental validation is carried out for the baseline case and the best Gurney flap configurations.

4. CASCADE AND GURNEY FLAP GEOMETRIES

The profile used for blades is T106 which is a high lift LP turbine blade profile, which was used by Stieger (2002). T106 blade is used in the mid span section of a Pratt and Whitney PW2037 rotor. The blade coordinates are openly available and extensive research work is done on T106 and its variants by many research groups around the world with respect to flow separation on this blade. Hence this profile is selected for the present investigation.

Figure 1 shows the T106 blade profile. Non-dimensional blade coordinates were extracted from Stieger (2002) and scaled them down based on the chord length of 60 mm used in the present case. Cascade specifications are shown in Table 1. Schematic of Gurney flaps used for computations are shown in Fig. 2. For the sake of clarity, only the trailing edge region of the blade is shown. The details of Gurney flaps are also shown in Table 2.

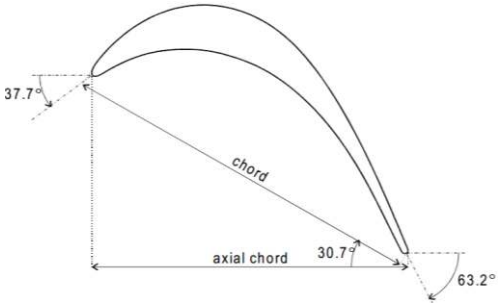

Fig. 1. T106 Blade Profile.

Table 1 T106 Design Data

Chord (Ch)	60 mm
Axial chord (Ch_X)	51.6 mm
Blade spacing, S	48 mm
Solidity (Ch/S)	1.25
Blade height, H	120 mm
Aspect ratio (H/S)	2
Inlet blade angle, α_{1b}	37.7^O
Blade stagger angle, γ	30.7^O
Exit blade angle, α_{2b}	63.2^O
Flow turning angle, ε	100.7^O
Zweifel loading coefficient, ψ_Z $=2S/Chx\,(\tan\alpha_{2b}-\tan\alpha_{1b})\cos\alpha_{2b}$	1.03

5. COMPUTATIONAL METHODOLOGY

The cascade geometry was modelled in AutoCAD. Domain consists of half flow passages on both the sides of the blade. The domain inlet is 1.5 chord upstream from the leading edge and the domain outlet is two chords downstream the trailing edge. The inlet and the outlet of the computational domain were placed far enough from the blade to create experimental conditions to the possible extent.

As ANSYS CFX does not support 2-D mesh, the computational 2D domain of the linear axial turbine cascade presented for all the simulations is 2.5D rather than 2D. In 2.5D, the whole 2D mesh is extended in the span wise direction by one mesh element thickness. An unstructured tetrahedral mesh was used for spatial discretization of the computational domain with prism layer elements along the walls to resolve boundary layers. The initial height and the number of prism layers have been chosen such that the minimum and maximum value of y^+ is always in the range of 0.001 to 1 respectively. The results of grid dependency studies are presented in Table 3. From these studies, medium grid is found to give results within 1% of those of fine grid. Hence this grid is used for all computations. Additional boundary-layer was achieved by clustering more tetrahedral elements close to wall surfaces. Various images of the domain and mesh for the baseline case and different Gurney flap cases considered are presented in Fig. 3.

All the simulations were carried out at steady state. Air was considered as the working fluid with constant kinematic viscosity of 1.6×10^{-6} m^2/s which corresponds to approximately the viscosity of air in experimental conditions in the laboratory.

Table 3 Details of grid used for meshing

Grid	No. of cells	ψ_{int}	Ratio of no. of cells	% Change in ψ_{int}
Coarse	0.205×10^6	0.0610	-	-
Medium	0.269×10^6	0.0671	1.31	10
Fine	0.315×10^6	0.0674	1.17	0.45

% Change in ψ_{int} is defined as the percentage change in ψ_{int} for the previous grid and present grid.

The following boundary conditions were applied for different boundaries of the computational domain. Velocity boundary condition was specified at the inlet and inlet turbulence intensity was set to 1%. Outlet boundary condition was set to zero static pressure. Blade surface was specified as no-slip wall. Translational periodic boundary condition was set between periodic 1 and periodic 2 surfaces. Translational periodicity boundary conditions are set to simulate linear cascade with infinite number of blades, ensuring periodicity in pitchwise direction.

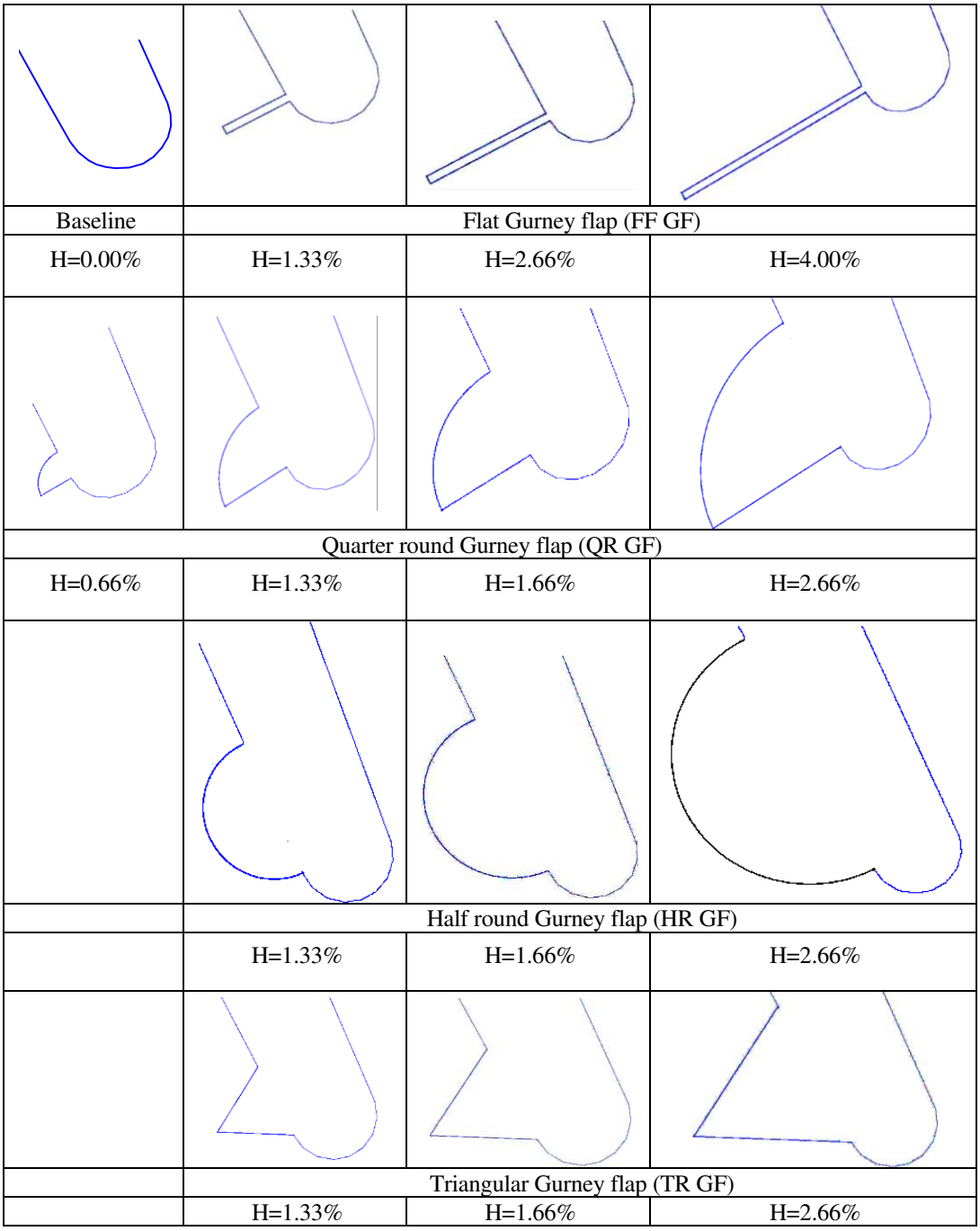

Fig. 2. Details of Gurney flaps for which computations are carried out.

Table 2 Gurney flaps tested

S. No.	GF Configuration	Height, H (Computations)	Height, H (Expts.)
1	Baseline	0.00%	0.00%
2	Flat (FF GF)	1.33%, 2.66% and 4.00%	1.33%
3	Quarter Round (QR GF)	0.66%, 1.33%, 1.66% and 2.66%	1.33%
4	Half Round (HR GF)	1.33%, 1.66% and 2.66%	-
5	Triangular (TR GF)	1.33%, 1.66% and 2.66%	-

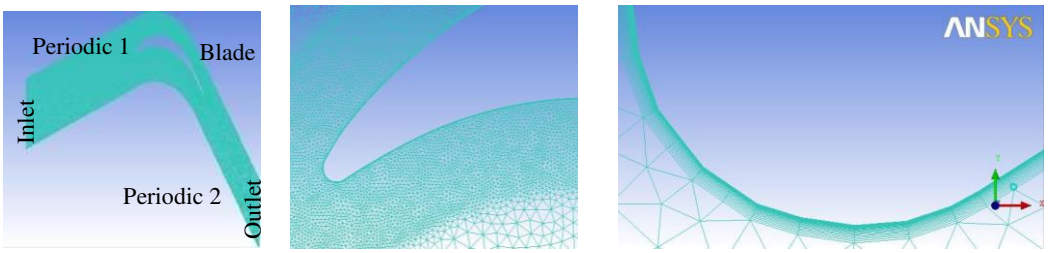

a) Entire domain b) Near blade surfaces c) Prism layer elements near leading edge

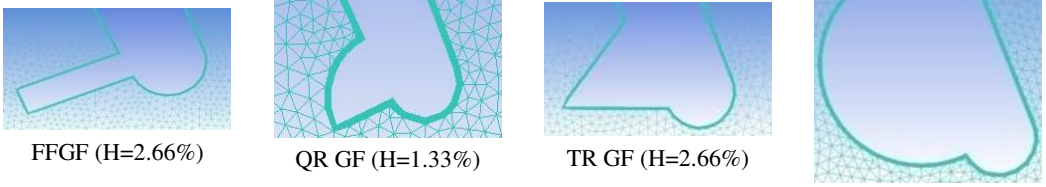

FFGF (H=2.66%) QR GF (H=1.33%) TR GF (H=2.66%) HR GF (H=2.66%)

Fig. 3. Computational grids for different types of Gurney flaps.

Taking into account the separation and the transition of the boundary layer on LP turbine blade, SST κ-ω turbulence model coupled with transition gamma-theta (γ–θ) model is used. SST κ-ω turbulence model was developed by Menter (1994). Original k-ω model of Wilcox (1993) in the inner region of the boundary layer was utilized. Standard k-ε model was used in the outer region and in free shear flows. This model is shown improvements in the prediction of adverse pressure gradient flows, which are common on the suction surface of turbine blades. Gamma-theta model was developed by Langtry and Menter (2005). It is based on two transport equations, one for intermittency and one for a transition onset criterion in terms of momentum thickness Reynolds number. This model allows the 1st order effects of transition to be included in everyday industrial CFD simulations.

The simulations were carried out till the residual values for mass and momentum equations were reduced to 10^{-6}.

6. EXPERIMENTAL METHODOLOGY

Experiments were carried out in a subsonic cascade tunnel (Fig. 4a) powered by a 150 HP motor. The motor is directly coupled to centrifugal fan which is capable of producing pressure rise of 2000 mm WC. The tunnel has a test section of 120 mm x 228 mm, which is capable of accommodating 6-7 blades.

A linear cascade (Fig. 4b) with seven blades is used with a spacing of 48 mm. Blade chord and span are 60 mm and 120 mm respectively. T106 LP turbine profile is chosen for the present investigation. This profile is extensively used by many investigators.

In order to maintain periodicity for the central blade, total pressure was measured in the pitchwise direction using the Pitot tube. The measurements were carried out for three blade spacings covering the central blade and two blades on the either side of the central blade and it was found that the flow was periodic.

The central blade was instrumented (Fig. 4c) for measurement of blade static pressure on both surfaces. A sub miniature four hole wake probe with minimum spatial resolution of 0.254 mm in the wake direction (Fig. 4d) was designed, fabricated and calibrated at four different Reynolds numbers. It was used to measure the pressures in the wake region downstream of the cascade blades from which exit velocity and its components, total and static pressures and flow angles can be obtained. A miniature Pitot tube with tip diameter of 0.254 mm was used to measure the total pressure upstream of the cascade. These measurements are used to calculate lift coefficient (C_L), total pressure loss coefficient (ψ), overall integrated loss coefficient (ψ_{int}) and flow deflection, ε.

FC012 Model 2 digital micromanometer with a range of ±200 mm WC and accuracy of ±0.1% full scale reading and two 20 channel selection boxes (Model FCO 91-3, Furness Controls Ltd., U.K.) were used for pressure measurements.

7. RESULTS AND DISCUSSION

Computations were carried out to study the effect of Reynolds number on the baseline case. The performance parameters chosen for analysis are static pressure distribution over a blade surface (static pressure distribution), total pressure loss coefficient (ψ) from wake survey, lift coefficient (C_L) and overall integrated loss coefficient (ψ_{int}). Computational analysis of cascade with Gurney flap attached to pressure surface of blade at trailing edge is carried out by systematically varying the height

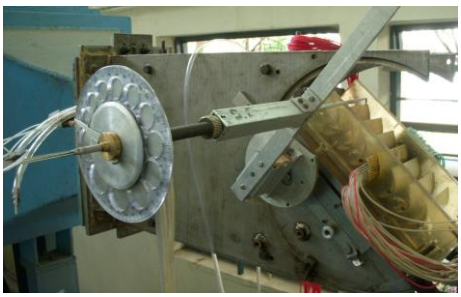

a) Subsonic cascade tunnel

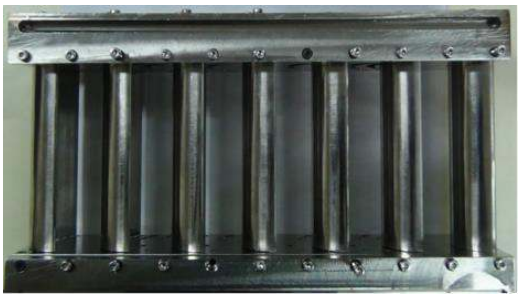

b) Linear cascade with 7 blades

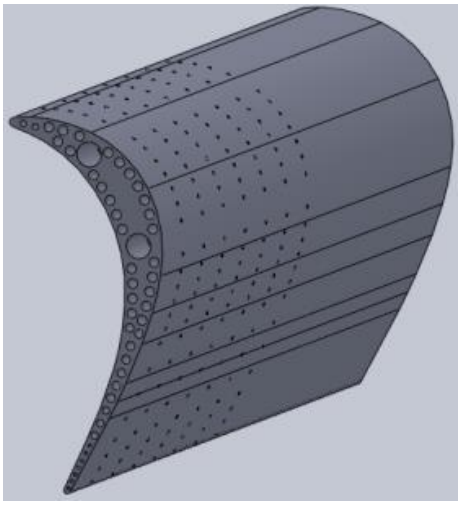

c) Instrumented blade

d) Four hole sub miniature wake probe

Fig. 4. Experimental facility, cascade, instrumented blade and wake probe.

and shape of Gurney flap. Based on the performance of the GF in comparison to baseline case, the best configurations are selected. Experimental validation is carried out for the baseline case and the best Gurney flap configuration cases.

7.1 Effect of Reynolds Number on Aerodynamic Performance of Baseline Case

The computations were carried out on baseline case with the objective of examining the effects of Reynolds numbers at low turbulence intensity (1%) for steady case. The computational results are presented in terms of static pressure coefficients on the blade surface, velocity vectors in the blade passage and total pressure loss at the cascade exit. Reynolds number for all the cases is based on inlet velocity and blade chord. Static pressure distributions on the blade surfaces for Reynolds number range, $37500 \leq Re \leq 138750$ at 1% inlet turbulence intensity are presented in Fig. 5. Figure 5a represents the validation of computational static pressure distribution distributions with the available experimental data (Stieger, 2002) based at the same exit Reynolds number (based on exit velocity and axial chord, Re=160000). Figure 5b shows static pressure distributions for five different Reynolds numbers. On the suction surface, there is a region of constant pressure distribution, which is known as plateau or terrace close to the aft end. This plateau represents the flow separation. The point where the static pressure distribution starts becoming constant is the point of separation. It can be seen from Fig. 5b, as Reynolds number is decreased, the point of separation on the suction surface is moving upstream. The size of plateau region increases with the decrease of Reynolds number indicating that of separation increases at low Reynolds numbers.

Stieger defined static pressure coefficient based on exit velocity. In the present work static pressure coefficient is defined on the basis of inlet velocity to compare static pressure distribution with and without Gurney flap. Only to compare with Stieger data, static pressure distribution based on exit velocity is shown in Fig. 5a.

Velocity vectors at three different Reynolds numbers are presented in Fig. 6. From velocity contours it can be seen that at higher Re=138750, the flow separates at a point very close to the trailing edge. For an intermediate Reynolds number of 75000, separation point moves upstream and the same trend continues with the decrease in Reynolds numbers. For the lowest Reynolds number of 37500, the separation begins much earlier than that of the higher Reynolds number. Hence profile losses are higher. It can be seen from velocity vector plots that the wake gets broader with decrease in Reynolds number and shifts towards the pressure surface of adjacent top blade.

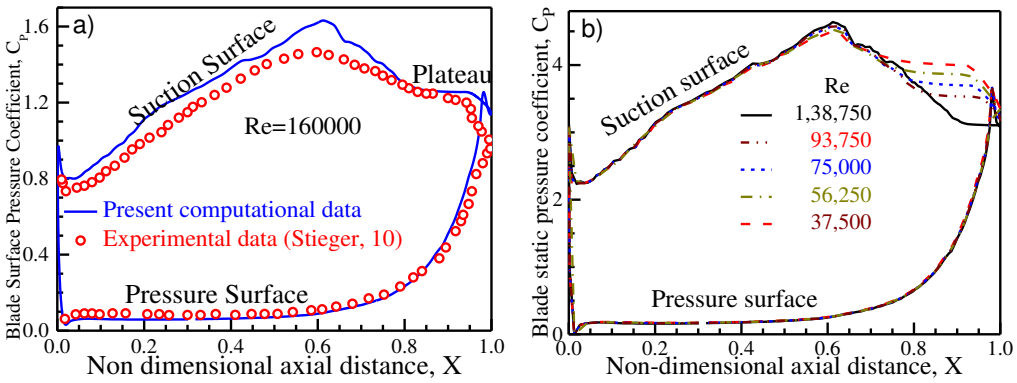

a) Comparison with Steiger's (2002) measurements b) Effect of Reynolds number

Fig. 5. Static pressure distribution on the blade surfaces of baseline configuration. Comparison of computational and experimental results Computational static pressure distributions: Effect of Reynolds number.

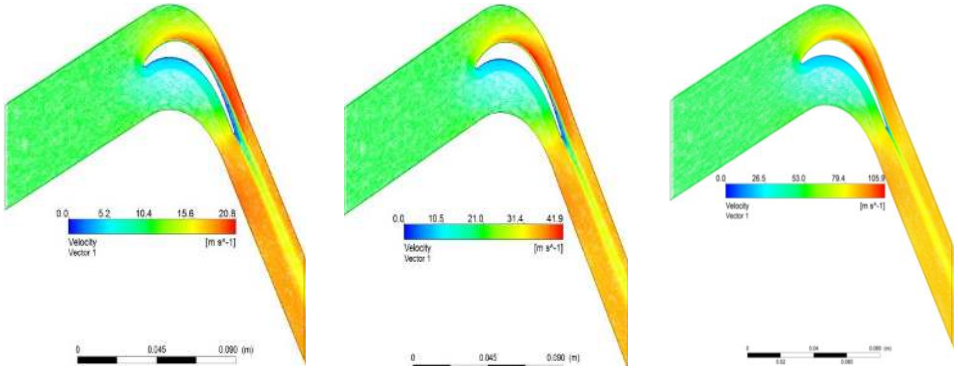

a) Re=37500 b) Re=75000 c) Re=138750

Fig. 6. Velocity vector plots for baseline configuration: Computational results.

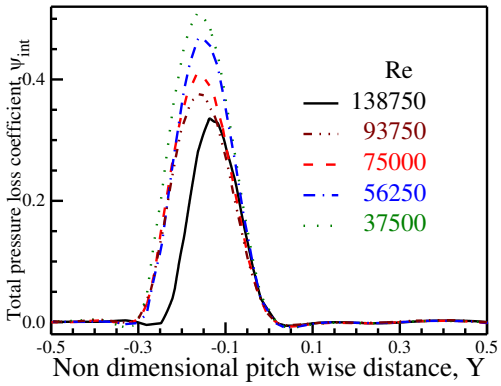

Fig. 7. Effect of Reynolds number on total pressure loss distribution: Computational results.

Total pressure loss coefficient (ψ_{int}) for one blade passage is shown in Fig. 7. With the decrease in Re, the wake region broadens and gets deeper indicating increase in the loss due to separation. Because of the flow separation, the wake centre tends to shift towards the pressure side of the next blade depicting large amount of flow separation at low Reynolds numbers. From Fig. 8, it can be seen that the overall integrated loss coefficient (ψ_{int}) at lowest Reynolds number is almost double as compared to that of the highest Reynolds numbers. The value of ψ_{int} keeps on decreasing with increase in Reynolds numbers.

7.2 Effect of Gurney Flap on Aerodynamic Performance of Axial Turbine Linear Cascade

The effect of Gurney flap is shown using static pressure distribution, velocity vectors and wake survey for five different Reynolds numbers similar to that of the baseline case. The flap considered for this comparison is 1.33% Ch Quarter Round. Figure 9 compares static pressure distribution for the baseline case and with flap. For a flap case, it can be seen that for all Reynolds numbers, static pressure distribution curve on the suction side overlaps over one another indicating a similar behaviour. Also the plateau region present for the baseline case representing separation has been completely eliminated in the case of flap concluding that flow sticks to the suction surface till the very end of trailing edge. Further, the area bounded between pressure and suction surfaces which represents the

lift coefficient (C_L) is always greater than that of the baseline case for all Reynolds number. Gurney flap increases the effective camber of airfoil which in turn is responsible for increase in lift coefficient, C_L.

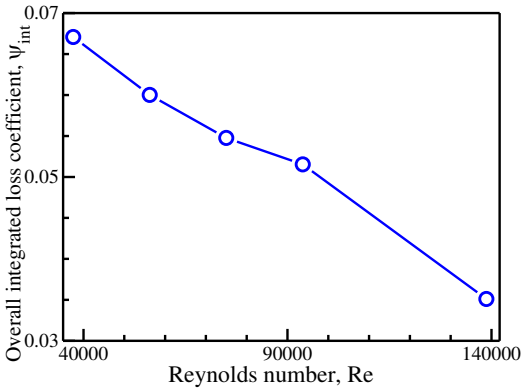

Fig. 8. Variation of overall integrated loss coefficient with Reynolds number: Computational results.

Figure 10 shows velocity vector plots with QR GF case for lowest Re=37500. It can be seen that because of the GF, flow accelerates and gets deflected towards the suction surface of the adjacent blade without getting separated. Because of the deflection of the mainstream by the GF, the adverse pressure gradient on the suction surface gets weakened thus resulting in thinning or elimination of separation bubble, delaying the transition onset, contributing to reductions of both the separation bubble generated loss and the turbulent boundary layer generated loss.

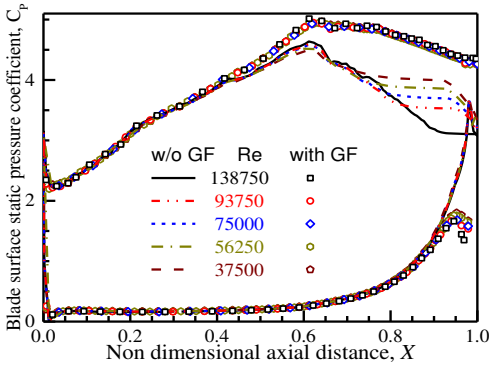

Fig. 9. Surface static pressure distribution for QR GF (H=1.33%): Computational results.

Figure 11 compares total pressure loss coefficient for one blade passage for baseline case and a case with flat GF of H=1.33%. With flaps, it can be seen that there is a shift of wake towards the suction side of the adjacent blade because of the increased flow deflection. Gurney flap apparently increases blade camber due to increased blade exit angle. Compared to baseline case, the wake depth has decreased substantially and for all Reynolds numbers, the wakes are almost overlapping with a minimal wake shift with the decrease in Reynolds number for the flap case.

It can be seen from Fig. 12, the overall integrated loss coefficient (ψ_{int}) for GF case is less than that of the baseline case at all Reynolds numbers. At the lowest Reynolds number, the difference between ψ_{int} for baseline case and GF case is highest. With increase in Reynolds number this difference in ψ_{int} decreases continuously.

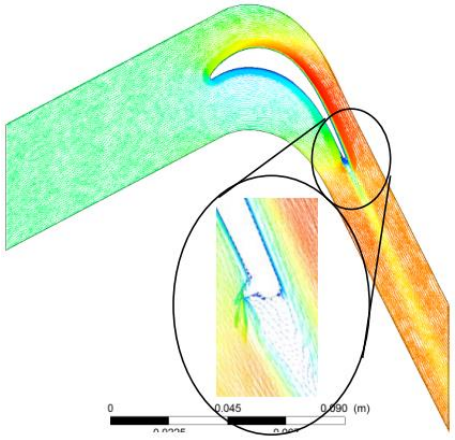

Fig. 10. Velocity vectors plot for QR GF (H=1.33%) at Re=37500: Computational results.

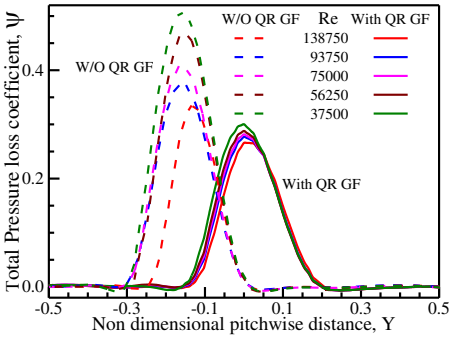

Fig. 11. Comparison of total pressure loss coefficient of QR GF (H=1.33%) with baseline case: Computational results.

Computational investigations of Gurney flap with different heights and with different shapes namely Flat (FF), Quarter Round (QR), Triangular (TR) and Half Round (HR) were carried out. The heights and shapes of Gurney flaps are presented in Table 2. The heights are systematically varied to identify the optimum GF height. Flat GF is commonly used GF. QR GF is similar to Flat GF, but expected for smooth fluid flow over the GF. Similarly HR and TR GFs are expected to allow the flow leave smoothly. Hence these shapes are chosen.

7.3 Effect of Gurney Flap Height on C_L, ψ_{int}, C_L/ψ_{int} and ε

Flat GF: Computations were carried out for three different heights of Flat GF cases. The heights include 1.33% Ch, 2.66% Ch and 4.00% Ch. The

effects of heights on various performance parameters are shown in Fig. 13.

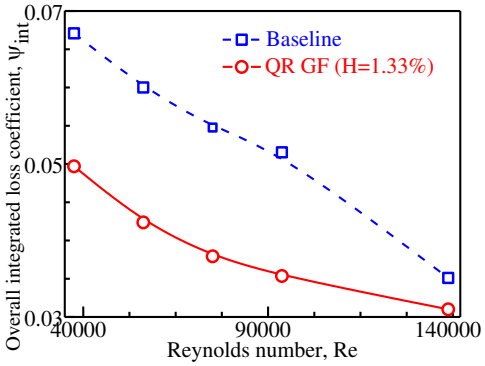

Fig. 12. Comparison of overall integrated loss coefficient of QR GF (H = 1.33%) with baseline case: Computational results.

From Fig. 13a, it can be seen with the decrease in Reynolds number, there is a slight increase in lift coefficient (C_L) for baseline case. For all the Gurney flap cases, it can be seen that lift coefficient (C_L) is always greater than that of the baseline case. With the addition of Gurney flap to the blade, the effective camber of the airfoil increases leading to increase in lift. With the increase in the height of the Gurney flap, lift coefficient (C_L) goes on increasing. For a particular height of GF, lift coefficient (C_L) is independent of Reynolds number.

If only lift coefficient (C_L) is considered as the criterion for selecting the optimum Gurney flap height, then one can conclude that the higher the height of the flap, better will be the performance, but losses also need to be taken into account before arriving at optimum Gurney flap height.

The variation of overall integrated loss coefficient (ψ_{int}) is shown in Fig. 13b. For the baseline case, ψ_{int} decreases with increase in Reynolds numbers. For 4.00% Ch Flat GF case, losses are higher than that of the baseline case for all Reynolds Numbers. In this case, though the flap is able to eliminate the laminar separation completely, the losses are still higher than that of the baseline case because height of the GF is very high which will induce losses more than that of the losses which it has eliminated by preventing laminar flow separation. The losses are mainly due to large increase in effective trailing edge radius. Hence it is necessary to choose the height of the Gurney flap judiciously.

For 2.66% Ch flat GF case, ψ_{int} is less than that of baseline case only at the lowest Reynolds number. In this 2.66% Ch flat GF case, losses almost remain constant for higher Reynolds numbers whereas losses decrease for baseline case with the increase in Reynolds numbers.

For 1.33% Ch flat GF case, losses are lower than that of the baseline case upto Re=120000. At lower Reynolds numbers, the losses in the GF case are much lower than that of the baseline case. With the increase in Reynolds number, the difference in losses between GF case and baseline case decreases. For Re>120000, GF needs to be retracted or Gurney flap becomes ineffective.

The ratio, C_L/ψ_{int} gives the combined effect of the lift coefficient and overall integrated loss coefficient on the cascade. We intend to have C_L as high as possible and ψ_{int} as low as possible with the flap case. Hence C_L/ψ_{int} should be as high as possible compared to that of the baseline case.

For 1.33% Ch flat GF case (Fig. 13c), the value of C_L/ψ_{int} is higher than that of the baseline case for large range of Reynolds numbers except that of the highest Reynolds number. The value of C_L/ψ_{int} for 1.33% Ch flat GF case is lot higher than that of the baseline case till Reynolds number becomes almost equal to 100000. At Re=130000 or so the value of C_L/ψ_{int} for the baseline case becomes higher than that of the 1.33% Ch flat GF case. It can be said 1.33% Ch flat GF gives good results for most part of the Reynolds number domain considered. Thus the performance of 1.33% Ch flat GF is better than that of the other two cases of GFs.

Figure 13d shows the variation of flow turning angle with Reynolds numbers for baseline case and three heights of flat GFs. The designed flow turning angle (equal to the blade camber angle, $\theta=\alpha_{2b}-\alpha_{1b}$) is 100.9^O. For the baseline case, ε is less than that of the blade camber angle of the blade because of the presence of laminar separation near the trailing edge. With the decrease of Reynolds number, ε for baseline case also decreases indicating large amount of separation. By the presence of the GF, flows turns more than that of the designed flows turning angle. With the increase in GF height, it can be seen that even the flow turning angle increases.

Half Round GF: In the flat Gurney flap case it is observed that the GF with height of 4% was capable to eliminate the flow separation completely as well as the lift produced by that case was maximum but the losses were too high making it impractical to use. Hence in the present case of Half Round GF, the different heights considered include 1.33% Ch HR, 1.66% Ch HR and 2.66% Ch HR. The effects of heights on various performance parameters are shown in Fig. 14.

Triangular GF: Computations were carried out for three different heights of Triangular GF cases. The heights include 1.33% Ch, 1.66% Ch and 2.66 % Ch. The effect of height on various parameters is shown in Fig. 15.

Quarter Round GF: Computations were carried out for four different heights of Quarter Round GF cases. The heights include 0.66% Ch, 1.33% Ch, 1.66% Ch and 2.66% Ch. The effect of height on various parameters is shown in Fig. 16.

Based on the above computations it is found that 1.33% Ch QR GF and 1.33% Ch Flat GF gives the best performance based on increased lift coefficient

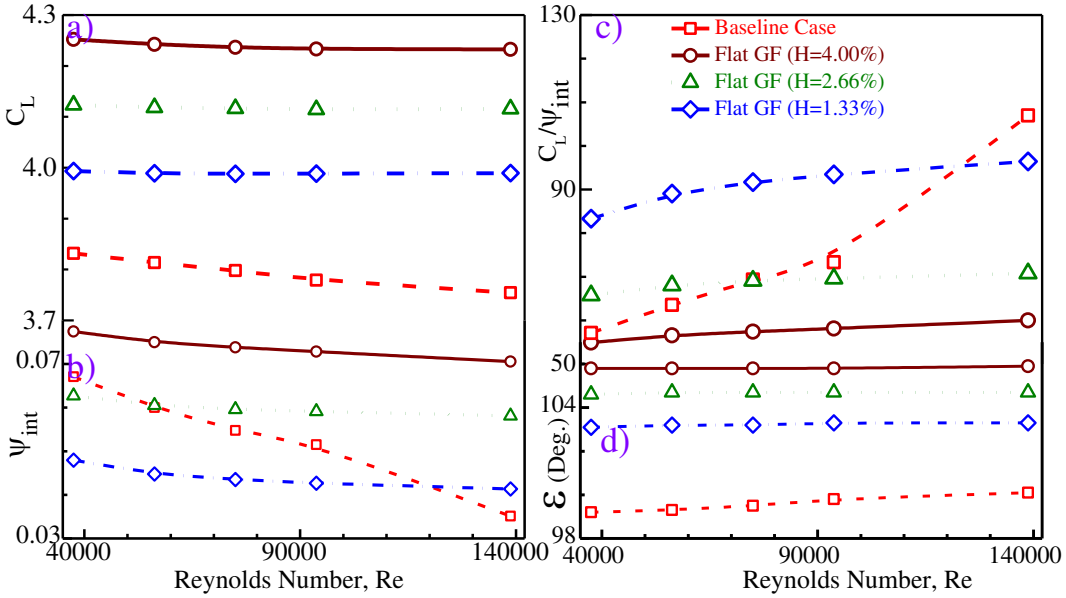

Fig. 13. Comparison of variation of performance parameters for different heights of Flat GF with baseline case a) C_L b) ψ_{int} c) C_L/ψ_{int} and d) ε: Computational results.

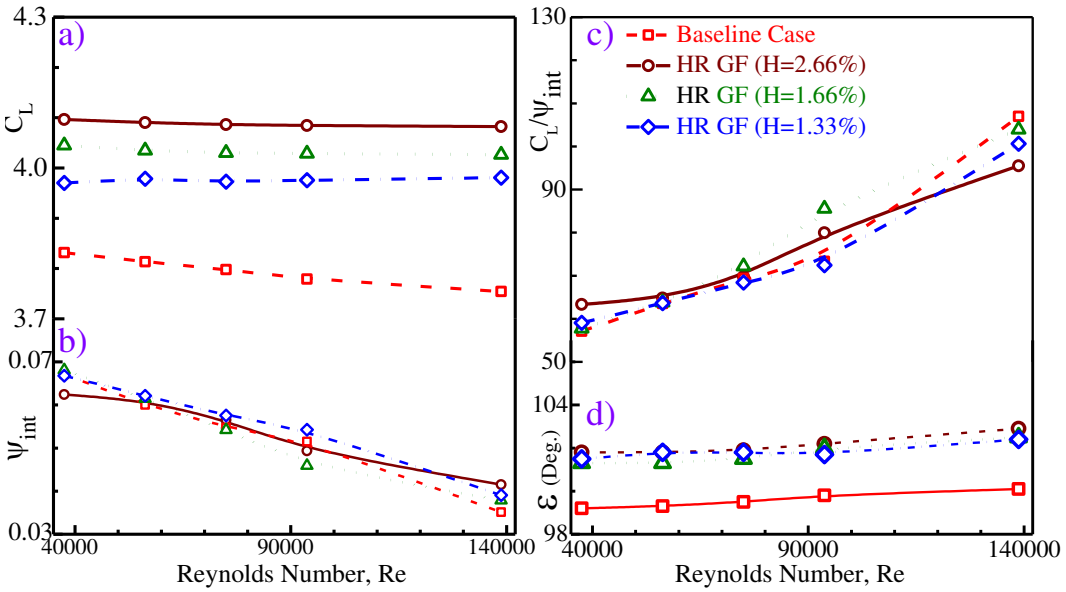

Fig. 14. Comparison of variation of performance parameters for different heights of HR GF with baseline case a) C_L b) ψ_{int} c) C_L/ψ_{int} and d) ε: Computational results.

(C_L) and overall integrated loss coefficient (ψ_{int}) in Reynolds number range considered. These two configurations were able to eliminate the separation completely (hence eliminate the laminar separation losses completely) as well as the losses produced by increase in effective trailing edge radius in these two cases are very low in comparison to that of the laminar flow separation losses in baseline case. For these two configurations, experimental validation was carried out and is presented below.

7.4 Optimum Gurney Flap Height

To find the optimum Gurney flap height, the following procedure is adopted. The ratio of lift coefficient to overall integrated loss coefficient, C_L/ψ_{int} is plotted against the height of Gurney flap. One such plot for Reynolds number of 37500 is shown in Fig. 17. From the figure, the optimum Gurney flap seems to be 1.66% for all configurations. However one has to cautious as the computations were carried out for only 3 or 4 Gurney flap heights. It is interesting to see that the variation of C_L/ψ_{int} is different for different GFs.

For flat GF, the value of C_L/ψ_{int} is increasing continuously as the height of GF is reduced. For HR

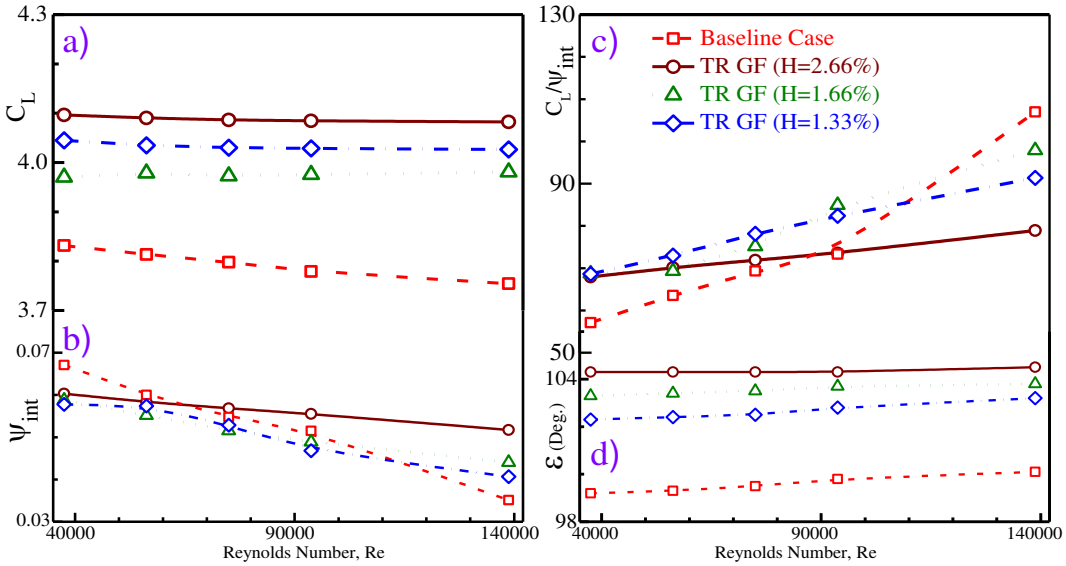

Fig. 15. Comparison of variation of performance parameters for different heights of TR GF with baseline case a) C_L b) ψ_{int} c) C_L/ψ_{int} and d) ε: Computational results.

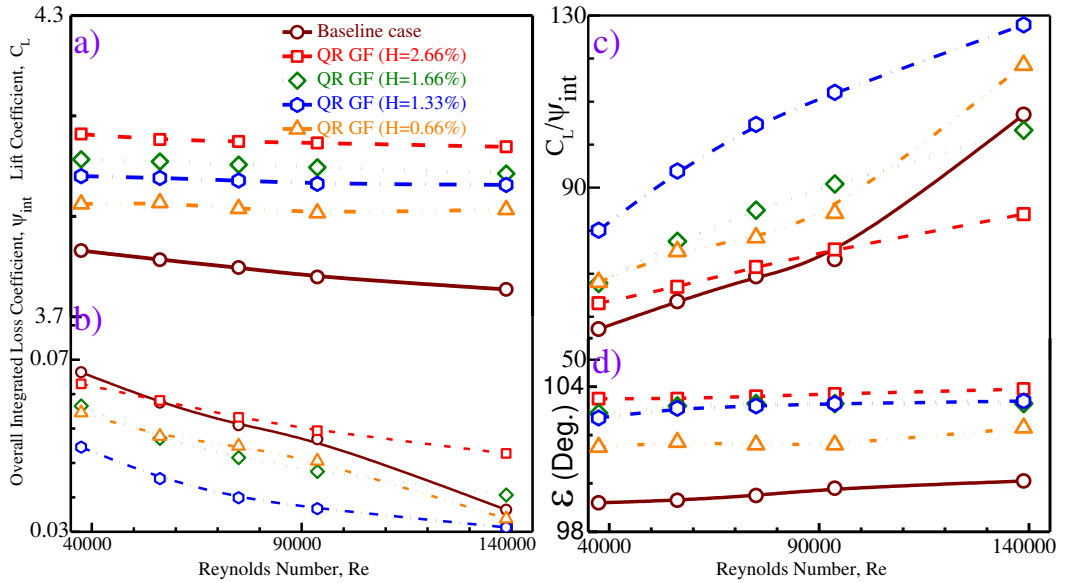

Fig. 16. Comparison of variation of performance parameters for different heights of QR GF with baseline case a) C_L b) ψ_{int} c) C_L/ψ_{int} and d) ε: Computational results.

GF, the value of C_L/ψ_{int} is decreasing continuously as the height of GF is reduced. For TR GF, the value of C_L/ψ_{int} is almost constant. For QR GF, the value of C_L/ψ_{int} is increasing continuously as the height of GF is reduced upto H=1.33%, then it decreases. Similar trends are observed at other Reynolds numbers (not presented here). Hence for both FF GF and QR GF, the optimum height may be taken as 1.33%. But FF GF gives larger value of C_L/ψ_{int} at the lowest Reynolds number. However at other Reynolds numbers (not presented here), QR GF gives larger value of C_L/ψ_{int}. Also shown is the value of C_L/ψ_{int} for baseline configuration without GF (H=0). This value is always lower than the corresponding values for all GFs except for FF GF of 4%.

The optimum height for QR GF at different Reynolds number is determined as follows. A quadratic equation is fitted for C_L/ψ_{int} with H as independent parameter. From the equation the optimum height can be determined by setting the derivative equal to zero and finding the optimum height.

$C_L/\psi_{int}=a+bH+cH^2$ $\quad d(C_L/\psi_{int})/dH=b+2cH=0$

for H_{opt} $b+2cH=0$ Hence $H_{opt}=-b/2c$

The values thus determined are shown in Fig. 18 as a tailed symbol along with the computed values for

QR GF at the five Reynolds numbers. They are also presented in Table 4.

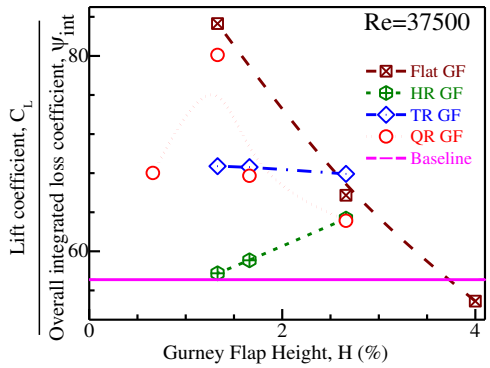

Fig. 17. Optimum height of Gurney flap at Re=37500: Computational results.

From the table, it is evident the optimum height decreases slowly as Reynolds number increases upto 93750. These values are close to H=1.33%, which is found to be optimal value for both FF and QR GFs. However, at Re=138750, the value of optimum GF height is very small. Also, the value of C_L/ψ_{int} for H=0 (baseline configuration) is shown as a straight line for the five Reynolds numbers. The colour of the straight line corresponds to Reynolds number of QR GF curves. The QR GF always gives higher value of C_L/ψ_{int} at all values of Reynolds number and heights of GF, except for GF with H=2.66% at Re=138750.

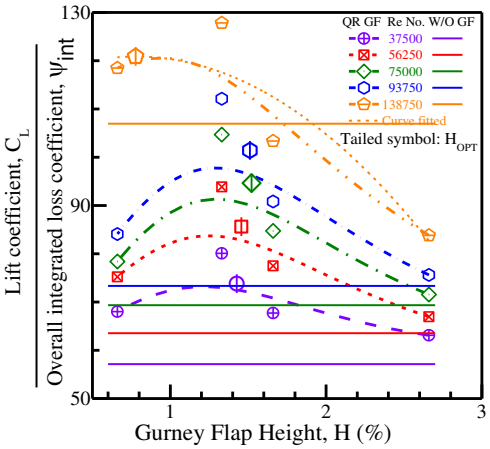

Fig. 18. Optimum height of QR Gurney flap at different Reynolds numbers: Computational results.

Table 4 Optimum height of QR Gurney flaps at different Reynolds Numbers: Computational results

Re	37500	56250	75000	93750	138750
H_{opt} (%)	1.450	1.389	1.389	1.384	0.962

7.5 Experimental Validation

Experiments were carried out for baseline case, 1.33% Ch Quarter Round GF case and 1.33% Ch Flat GF case in a linear cascade tunnel as described earlier using a cascade of seven blades. The height of Gurney flap is chosen as 1.33%, as the height of available Flat and QR GFs is 0.8 mm (H=1.33%) and this value is very close to the optimum height at the three middle values of Reynolds number. Instrumented blade is used to measure pressure distribution over the blade surface in order to capture separation. A sub miniature four hole wake probe was traversed to measure the exit flow in the wake region. Inlet conditions were measured using Pitot tube and static tappings on the side plates.

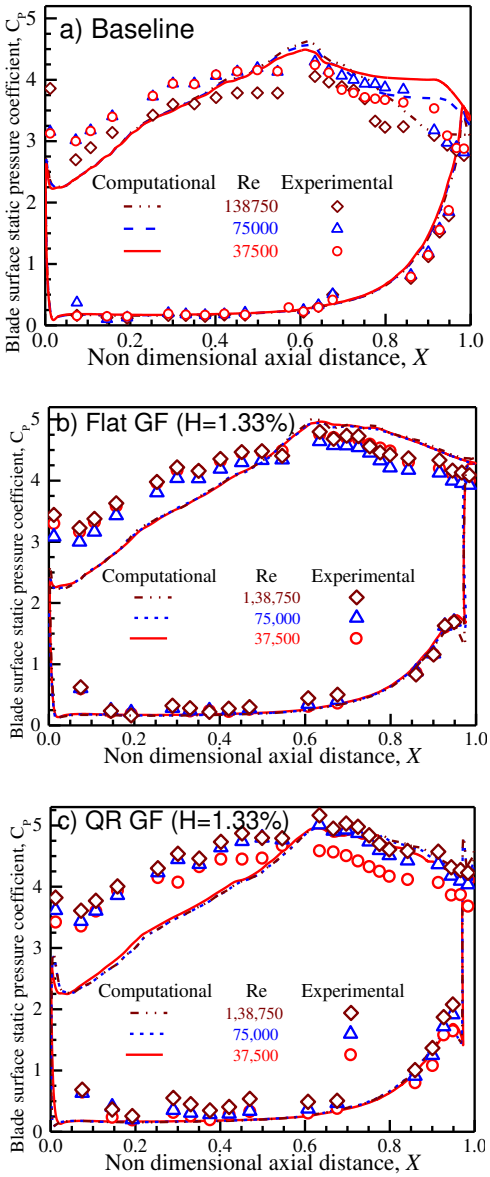

Fig. 19. Comparison of experimental and computational blade surface static pressure distribution for baseline cascade, cascade with FFGF (H=1.33%) and QR GF (H=1.33%).

Static Pressure Distribution for Baseline Cascade: The experimental and computational static pressure distribution for the baseline cascade presented in

Fig. 19a. For the sake of clarity the static pressure distributions are presented at three Reynolds numbers only, at 138750 (highest Re no.), 75000 (middle Re no.) and 37500 (lowest Re no.). From the figure, it can be seen that suction peak is reached at almost the same point for both computationally and experimentally distributions at all Reynolds numbers. The experimental separation was successfully captured in the aft portion of the suction surface of blade. The measured separation region is slightly smaller than that of the computed separation region.

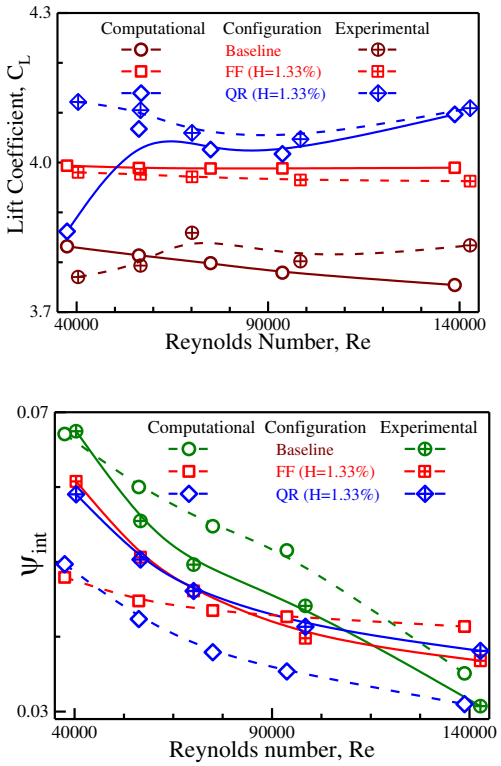

Fig. 20. Comparison of experimental and computational lift coefficient (C_L) and overall integrated loss coefficient (ψ_{int}).

The computations were carried out at exactly zero incidence, whereas for experiments it is difficult to measure incidence accurately. It is a known fact that angle of incidence does have an effect on static pressure distribution. A small difference in incidence angle is the reason for slight over prediction of static pressure distribution using computations in comparison to experiments. Even the accuracy with which the blades are fabricated does have an effect on static pressure distribution.

Static Pressure Distribution for Cascade with Flat Gurney Flap (H=1.33%): The experimental and computational static pressure distribution for 1.33% Ch Flat Gurney flap at five different Reynolds numbers are compared in Fig. 20a. It can be seen that both computationally and experimentally, the suction peak for all Reynolds numbers is reached at the same axial location corresponding to *X*=0.60. For all Reynolds numbers, the experimental static pressure distribution values are almost overlapping over one another.

Static Pressure Distribution for Cascade with Quarter Round Gurney Flap (H=1.33%): Experimental and computational static pressure distribution for 1.33% Ch Quarter Round Gurney Flap at five different Reynolds numbers are compared in Fig. 20b. The trends for this case are almost similar to that of 1.33% Ch Flat case. The only notable difference is the value of static pressure distribution on suction surface for 1.33% Ch QR GF is slightly higher than that of the 1.33% Ch Flat GF.

Experimental and computational lift coefficient (C_L) and experimental and computational overall integrated loss coefficient are compared in Fig. 20. The agreement between experimental and computational values is good.

8. CONCLUSIONS

An extensive computational investigation is carried out on separation control of low pressure turbine cascade using Gurney flaps of different configurations and different heights at five Reynolds numbers. From these investigations optimum configuration and heights of Gurney flap are identified. Experimental investigations are carried out on the cascade with these optimum values to validate the computational results. The following major conclusions are drawn:

For the baseline case (without GF), the region of laminar flow separation was successfully captured in both experimental and computational cases. For the baseline case, it was seen that with the decrease in the Reynolds number, the separation point starts moving upstream on the suction surface indicating the increase in separation losses. The shift in separation point was captured both experimentally and computationally from blade surface static pressures. Gurney flaps were able to eliminate separation completely but the height and shape of the Gurney flap has to be judiciously chosen. Lift coefficient (C_L) with Gurney flaps was always greater than that of the baseline case. The lift coefficient (C_L) increased with the increase in Gurney flap height, but the increased flap height increased in losses due to effective increase in trailing edge radius.

At low Reynolds numbers, overall integrated loss coefficient (ψ_{int}) for Gurney flap case with height greater than 1.66% Ch is higher than overall integrated loss coefficient (ψ_{int}) for baseline case irrespective of the shape of the flap.

The performance of all the Gurney flap shapes (Flat, Quarter Round and Triangular except Half Round) with a height of 1.33% Ch is better than that of the baseline case. All the three shapes of Gurney flaps were successful in eliminating the separation bubble completely. Thus the performance of Gurney flap with height of 1.33% Ch is superior to all other heights considered. Among the three Gurney flap shapes of height=1.33% Ch, Quarter Round and Flat Gurney flaps perform better than

that of the Triangular GFs. For these two shapes and the baseline case, computations were validated using cascade tunnel cascade experiments. The agreement between experimental and computational results is good.

For the baseline case as the Reynolds number increases, the laminar separation is not present and the flow remains attached to the suction surface till the trailing edge. Hence it can be concluded that the Gurney flap needs to be deployed at low Reynolds numbers and needs to be retracted at higher Reynolds numbers.

ACKNOWLEDGEMENTS

The authors would like to thank Mr. M. Veera Raghavan and Mr. N. Giri of Turbomachines Laboratory, Department of Mechanical Engineering, IIT Madras for fabricating the four hole sub miniature wake probe and for help in calibrating the probe and in the operation of the cascade tunnel.

REFERENCES

Banieghbal, M. R., E. M. Curtis, J. D. Denton, H. P. Hodson, I. Huntsman, V. Schulte, N. W. Harvey and A. B. Steele (1995). Wake passing in LP turbine blades. 85th Symposium on Loss Mechanisms and Unsteady Flows in Turbomachines, May 8-12, 1995, Derby, UK.

Byerley, A. R., O. Stormer, J. W. Baughn, T. W. Simon, K. W. Van Treuren and J. List (2003). Using Gurney flaps to control laminar separation on linear cascade blades. *ASME Journal of Turbomachinery* 125(1), 114-120.

Chen, P. P., W. Y. Qiao, H. L. Luo and A. H. Farhan (2010). Investigation of low solidity LP turbine cascade with flow control: Part 1– Active Flow Control Using Jet Flap. *ASME Paper* No. GT-2010-22328.

Curtis, E. M., H. P. Hodson, M. R. Banieghbal, J. D. Denton and R. J. Howell (1997). Development of blade profiles for low pressure turbine applications. *ASME Journal of Turbomachinery* 119(3), 531-538.

Dundi, T. M. K., N. Sitaram and M. Suresh (2012). Application of Gurney Flaps on a Centrifugal Fan Impeller. Paper No. O12008S, *International Journal of Fluid Machinery and Systems* 5(2), 65-71.

Lake, J. P., P. I. King and R. B. Rivir (1999). Reduction of separation losses on a turbine blade with low Reynolds numbers, AIAA Paper 1999-0242, 37th AIAA Aerospace Sciences Meeting and Exhibit, Jan. 11-14, 1999, Reno, NV, USA.

Langtry, R. B. and F. R. Menter (2005). Transition Modeling for General CFD Applications in Aeronautics. AIAA Paper 2005-522, 43rd AIAA Aerospace Sciences Meeting & Exhibit, January 10-13, 2005, Reno, NV, USA.

Menter, F. R. (1994). Two Equation Eddy Viscosity Turbulence Models for Engineering Applications. *AIAA J*ournal 32(8), 1598-1605.

Nilavarasan, T., N. G. Joshi and S. Chandel (2019). Effect of Gurney Flaps on the aerodynamic characteristics of NACA 0010 Cascades. *International Journal of Turbo and Jet Engines.*

Sharma, O.P. (1998). Impact of Reynolds number on low pressure turbine performance. *NASA CP 1998-206958*. 65-70.

Sondergaard, R., R. B. Rivir and J. P. Bons, Jeffrey (2002). Control of low-pressure turbine separation using vortex generator jets. *AIAA Journal of Propulsion and Power* 18(4) 889-895.

Stieger, R. D. (2002). *The effects of wakes on separating boundary layers in low pressure turbines*. Ph. D. Thesis, Cambridge University, UK.

Suresh, M. and N. Sitaram (2019). Effect of Gurney flap configuration on the performance of a centrifugal fan. *Journal of Applied Fluid Mechanics* 12(2) 565-571.

Volino, R. J. (2003). Passive flow control on low-pressure turbine airfoils. *ASME Journal of Turbomachinery* 125(4), 754-764.

Volino, R. J. and M. Ibrahim (2012). Separation control on high lift low-pressure turbine airfoils using pulsed vortex generator jets. *Applied Thermal Engineering* 49, 31-40.

Wang, J. J., Y. C. Li and K. C. Choi (2008). Gurney flap-Lift enhancement, mechanisms and applications. *Progress in Aerospace Sciences* 44(1), 22-47.

Wilcox, D. C. (1993). Comparison of Two-Equation Turbulence Models for Boundary Layers with Pressure Gradient. *AIAA Journal* 31(8), 1414-1421.